SAR Compliance Simulation Report for iPhones
V1.0.0

Model No.	FCC ID
A3260	BCG-E8948A
A3516	BCG-E8954A
A3517	BCG-E8955A
A3518	BCG-E8956A

Date of Simulation:
04/15/2025-06/15/2025
Location:
Apple Inc., Cupertino, CA, USA

Table of Contents

List of Figures:

List of Tables:

1 Introduction

This report demonstrates RF exposure compliance using SAR simulation for 2025 iPhone models (FCC IDs: BCG-E8947A, BCG-E8951A, BCG-E8952A, BCG-E8953A). The wireless power transfer (WPT) module on 2025 iPhones, in addition to being charged by a desktop and portable WPT charger (puck), also support WPT charging function at 360 kHz to charge accessories. This report presents the evaluation of SAR and E-field induced inside a human tissue when the iPhone is wirelessly charging potential external accessories.

To demonstrate RF exposure compliance for 2025 iPhones at 360 kHz operating frequency, as permitted by §2.1093 (certification for portable devices below 4 MHz), SAR numerical simulations are performed to demonstrate compliance to the 1.6 W/kg localized 1-g SAR limit.

Currently, the charging session only occurs when the phone is connected to an AC power outlet. However, due to the potential apple accessories in future and the phone being held in place by magnets, it is envisioned that customers may use the charging function in a portable use condition, for example, charging the battery while making a call or texting. Therefore, to be conservative we evaluate iPhone WPT transmitter as a mixed mobile/portable device. Future designs and accessories may support true portable use condition, with the host-client pair able to be placed in a pocket or backpack. In those cases, a body-worn exposure assessment would be conducted.

The following sections describe the modeling, measured H-field, simulated H-field, and simulated SAR.

2 Wireless Power Transfer System

The wireless power transfer system consists of a transmitting coil with 13 turns and measures 9.06 μH nominally in free air. The coil is wound spirally and made of stranded wire. Below are the details of the Phone (Tx) coil which is used in all the iPhone models described in section 1 of the report.

Tx Coil Winding Type	Spiral, 1 Layer, Stranded Wire
Turns	13
Inner Radius	10.06 mm
Outer Radius	21.35 mm
Cross-section	Rectangular
Thickness	0.13 mm
Width	0.62 mm

Rx Coil Winding Type	Spiral, 1 Layer, Stranded Wire
Turns	11
Inner Radius	10.9 mm
Outer Radius	18.9 mm
Cross-section	Rectangular
Thickness	0.32 mm
Width	0.49 mm

Below are some key initial parameters used in the design that will be helpful in determining worst-case use for exposure: These are common to all the iPhone models described in section 1 of this report.

Table 1. Key design parameters

Item	Description
Max Power	7.5 W
Functional On-body max offset	Refer to the graph below*
Operating Frequency	f_0 = 360 kHz
Communications/Modulation Method	FSK -> Phone to Accessory ASK -> Accessory to Phone
Object Detection Mode	Magnetic + NFC

* Refer to antenna location file for all antennas in the phone, and how the WPT coil is separated from other antennas.

3 SAR Simulations Methodology

The following steps has been taken to show the validity of the model used for SAR Simulations:

1) EM Simulation:
   a. Import a CAD model that represents the actual product in the simulation tool.
   b. Define material properties inside the product based on vendor's inputs.
   c. Extract two-port network impedance matrix ([Z]) from the simulation.
2) Circuit Simulation:
   a. Include the impedance matrix in the wireless power transfer (WPT) circuit model.
   b. Run circuit simulation and extract coils' current waveforms.
3) Field Calculations:
   a. Use the current waveforms to drive the EM simulation model.
   b. Calculate H-field from the simulation.
4) Validate Simulation Model:
   a. Measure H-field, and compare with simulation result
   b. Perform full uncertainty analysis
   c. Once a correlation is established, and model's accuracy is verified, this model will be used for computational exposure assessments (e.g., SAR simulations).

The entire workflow is summarized and shown in Fig. 1.
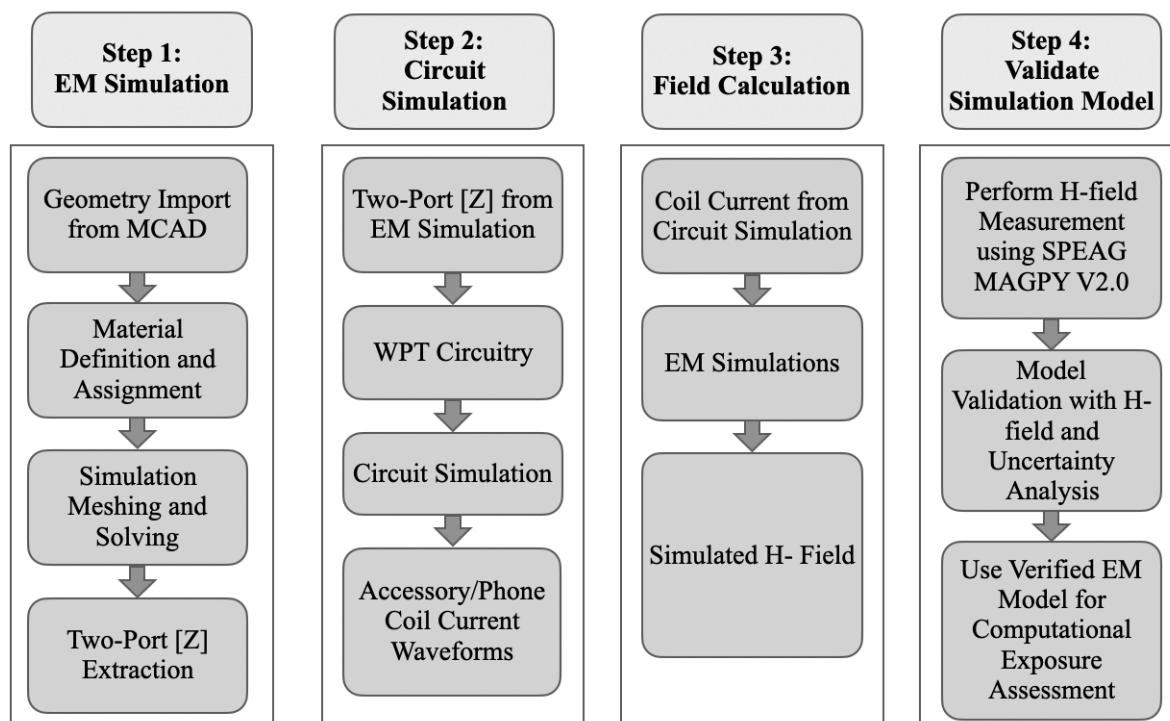
Figure 1: Model validation workflow for computational exposure assessment

4   H-field Simulations for Transmitter

The Electromagnetics simulations are conducted using commercially available software ANSYS HFSS. To validate the simulation model, H-field measurements are made on the EUT (as explained above) and compared to the simulated model results. The validated model is then used for SAR simulations.

SPEAG Magnetic Amplitude and Gradient Probe System (MAGPy) V2.0 probe shown in Fig. 2 is used to measure the H-field. This probe is mounted on DASY8 robotic system. The probe consists of 24 small loop sensors arranged on the corners of a 22mm cube used for measuring H-field amplitude and gradient. The lower measuring loops are 7.5mm from the probe tip enabling a closer measurement to the electromagnetic source. The probe also has two dipoles and a monopole to measure the E- field. Probe specifications are described in Table 2.
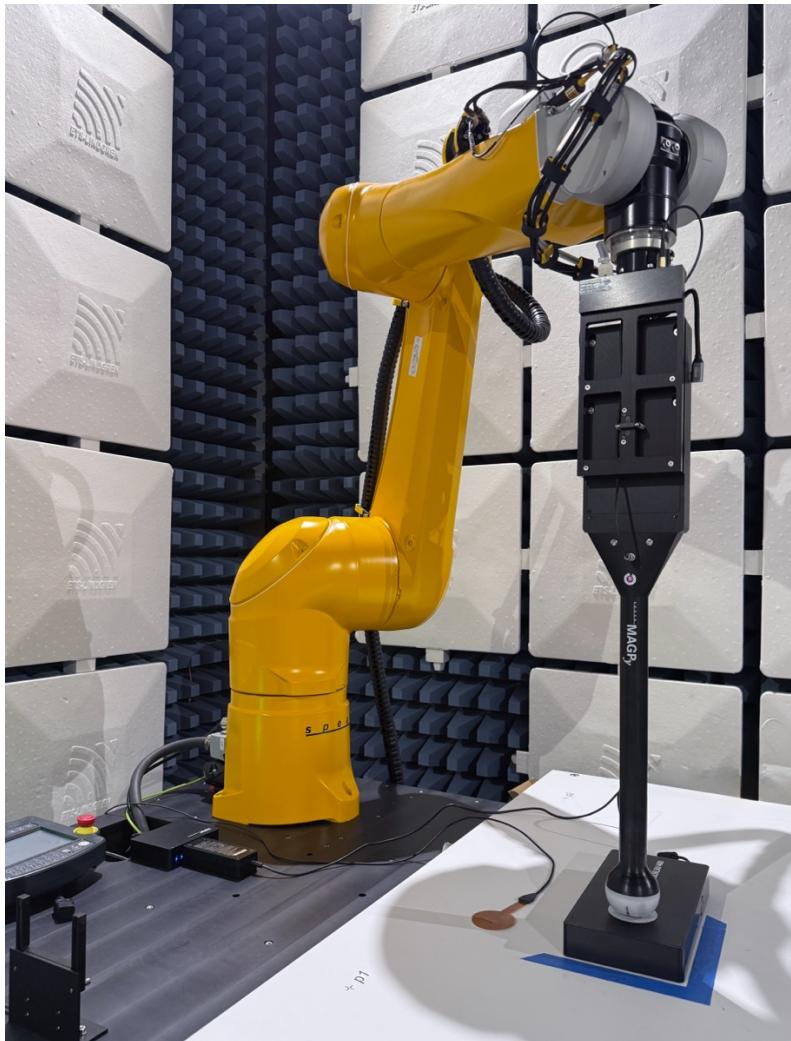
Figure 2: SPEAG DASY8 system with MAGPy V2.0 measurement probe

Table 2. Probe Specifications:

Model	MAGPy V2.0
Frequency	3 kHz – 10 MHz
Measurement Center	18.5 mm from the probe tip
Dimensions: (H-field sensor loop size) (E-field sensor arm length) (Overall Diameter)	1 cm² 50 mm 60 mm
Dynamic Range	0.08 to 2000 V/m for Electric field 0.1 to 3200 A/m for Magnetic field
Combined uncertainty	0.64 dB
Extended uncertainty ($k=2$)	1.3 dB
Application	Electric and Magnetic field measurement

For the simulation-measurement correlation study, the direct exposure case where only the iPhone (TX) is present is chosen. The measurement setup is shown in Fig. 3. As shown in the measurement setup, the center of probe coils is 18.5 mm away from the true 0 mm touch position and lower four sensor are 7.5mm away. Following procedure was used to compute the averaged fields from simulation results for correlating with measured data: The volumetric H-field is exported from HFSS and post-processed using a MATLAB script to include the SPEAG MAGPy V2.0 probe averaging effect. To accurately measure the H-field as close to the DUT as possible, the lowest sensor positioned at 7.5 mm away is utilized for correlation purposes. The operation of the robotic DASY8 system necessitates a 0.05 mm offset to prevent collisions between the probe and the DUT. Each of the eight MAGPy V2.0 probe sensors consists of three internal loops. These loops measure orthogonal H-field by integrating it over their effective aperture area. It is to be noted that the script disregards any potential loading effect that the probe may exert on the DUT, including mutual interaction with the DUT coils. Based on our experience, this mutual interaction is partially responsible for the discrepancy observed between the simulation and measurement outcomes when the probe is in contact with the DUT.
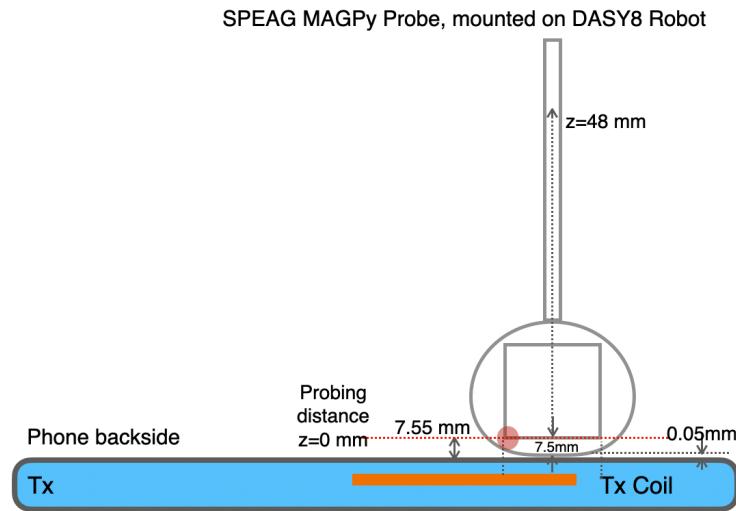
Figure 3: H-field measurement setup for direct exposure case

Simulation and measurement correlation is performed at a vertical distance away from the DUT and the probe is moved vertically in Z direction from 0 mm (sensor center) with the step size of 2 mm till 25 measurements are taken.
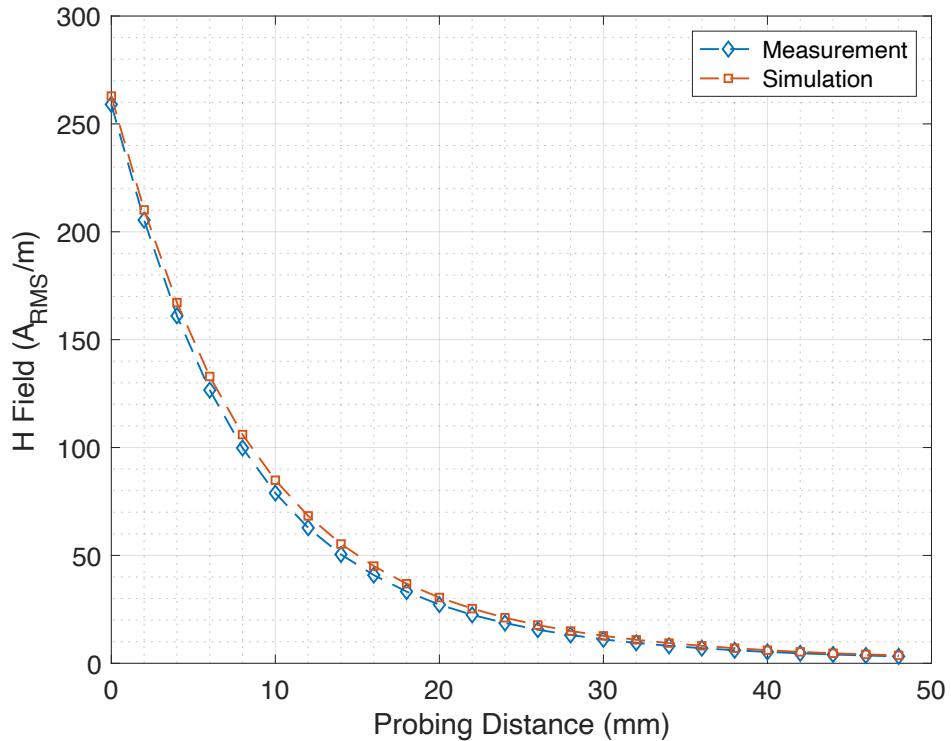

Figure 4: Simulation vs. measured H-field comparison for direct exposure case

The above Fig. 4 shows good correlation between the measurements and simulations. At distance very close to the DUT, simulations are little more conservative than measurements. This validated simulation model is then used for SAR simulations in the next sections.

5 SAR Simulations

The validated simulation model is used for SAR calculations with a phantom added in contact with the EUT. The simulations are computed on a 40 core CPU server with an available RAM of 2Terabytes. For this simulation, the model run takes approximately 6 hours to complete. The following steps are used for accurate SAR calculations:

1) Elliptical phantom used in body exposure measurements is commercially available from SPEAG: Outer Dimensions of 600mm x 400mm x 150mm.
2) Homogeneous tissue material is used as liquid for desired frequency.
3) Power loss in phantom is calculated.
4) Divide power loss by mass density to calculate SAR.

$$SAR = \frac{P_l}{\rho}$$

$$P_l = \text{Power loss density}$$

$$\rho = \text{Mass density}$$

5) Point SAR is averaged over 1g or 10g tissue.
6) For SAR simulations, mass density of 1000 Kg/m^3 is used for the Phantom.

Human Tissue Material Properties at 360 kHz:

The worst-case scenario has been identified to be when a user is holding the device in hand and taking a call or holding the phone on their body while charging. For the homogenous SAR phantom, with the following electrical properties is used in the simulations.
Electrical Properties:

Table 3: Electrical properties for SAR phantom

Mass Density (Kg/m^3)	Permittivity	Conductivity (S/m)
1000	55	0.75

Mesh Adaptation:
HFSS adapts the mesh based on field strength. It is important to ensure the mesh is refined to capture SAR accurately. This can be done by using adaptive meshing available in HFSS and mesh refinement process is described in Fig. 5.
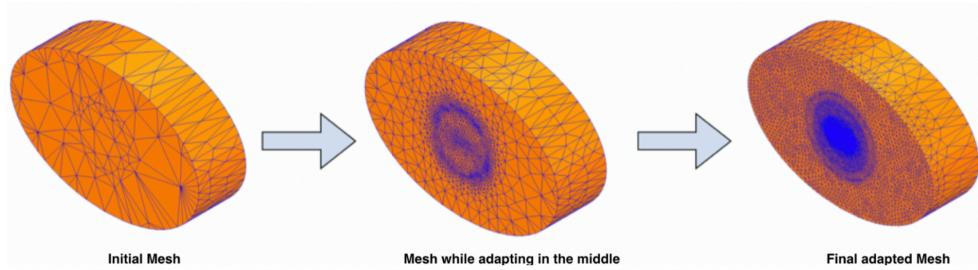
Figure 5: Initial mesh generation and then refinement through adaptive meshing technique in HFSS

SAR Results:

For the SAR investigation of the iPhone (Tx) characterized by a flat surface in wireless power transfer region, a conservative (worst-case) exposure scenario is considered for assessment purpose.

In this case, the iPhone (Tx) is in direct contact with the Phantom and no accessory present exposing the phantom with the worst-case exposure possible. For this evaluation, the iPhone (Tx) is excited with the maximum current that the Tx is capable of supplying to the accessory (Rx) in the case of worst-case alignment.

Adherence to this worst-case scenario will ensure that the exposure remains within the permissible limits for all Tx-Rx operating configurations.

Model number	Description	Peak Spatial Average SAR (W/kg) Averaged over 1 gram	Peak Spatial Average E-field (V/m) Averaged over 2x2x2 mm³
A3260, BCG-8948A; A3516, BCG-8954A; A3517, BCG-E8955A; A3518, BCG-E8956A		0.031	20.97

SAR plot is shown in Fig. 6 for the worst-case direct exposure.
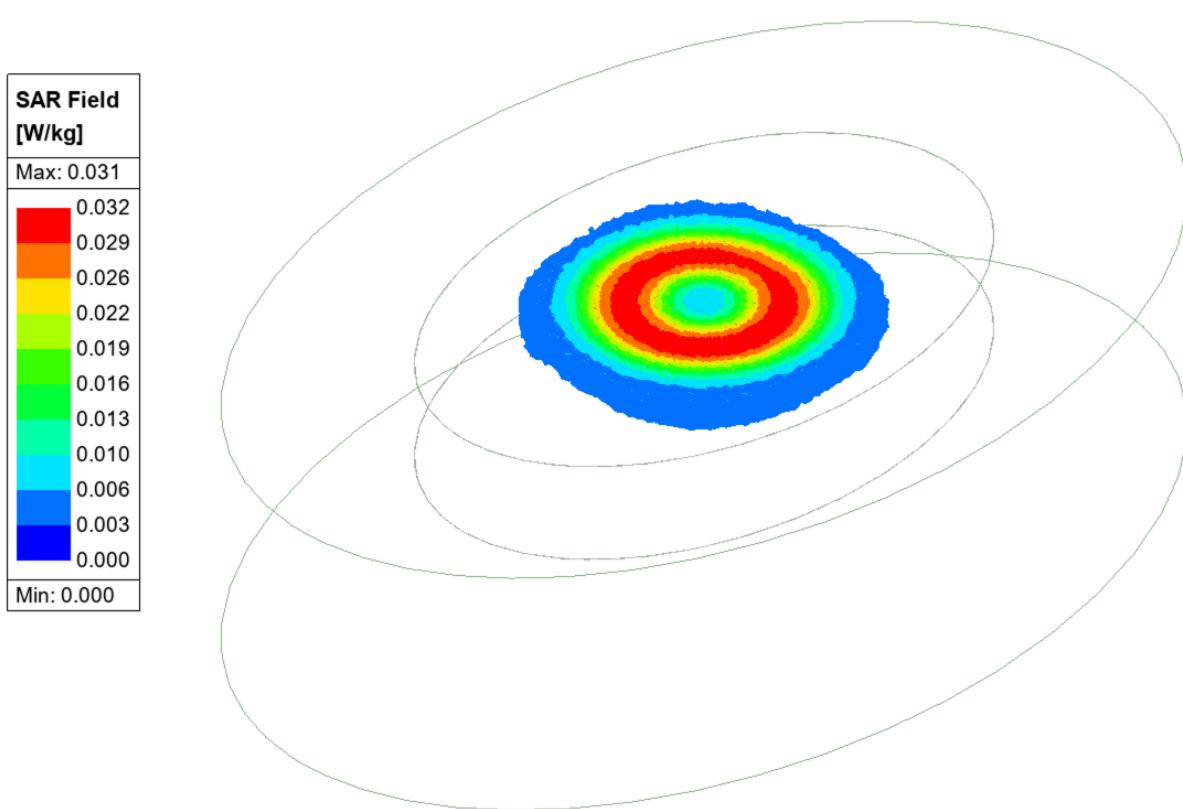
(a) Average SAR plot for direct exposure Case
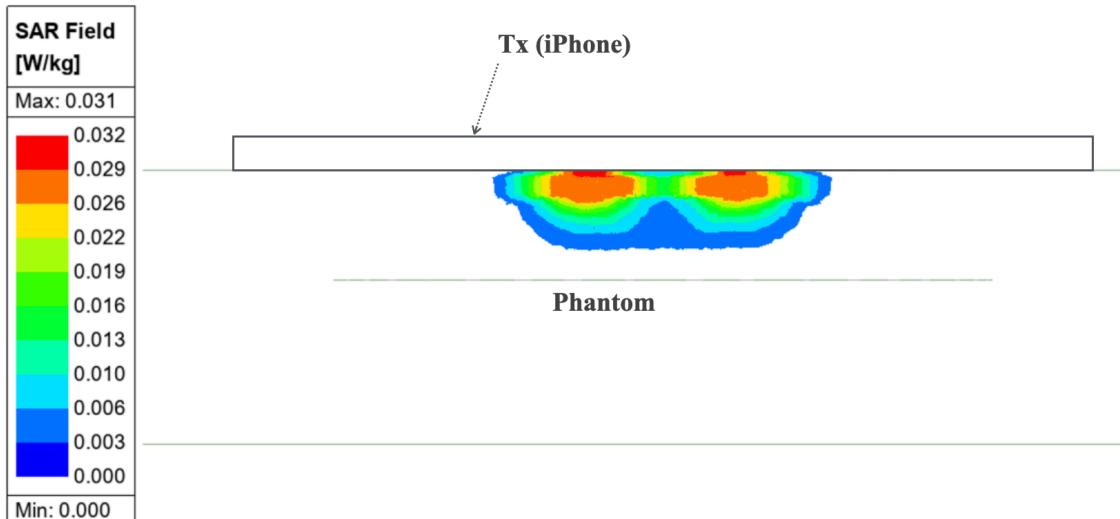
(b) Side view of average SAR plot for direct exposure Case

Figure 6: Spatial 1-gram average SAR, (a) full view, (b) side view

E-field distribution inside the phantom is shown below. Please note that the value reported in the table above was averaged over a cube of 2mmx2mmx2mm and that explains why the value is lower than the peak E-field in this plot.
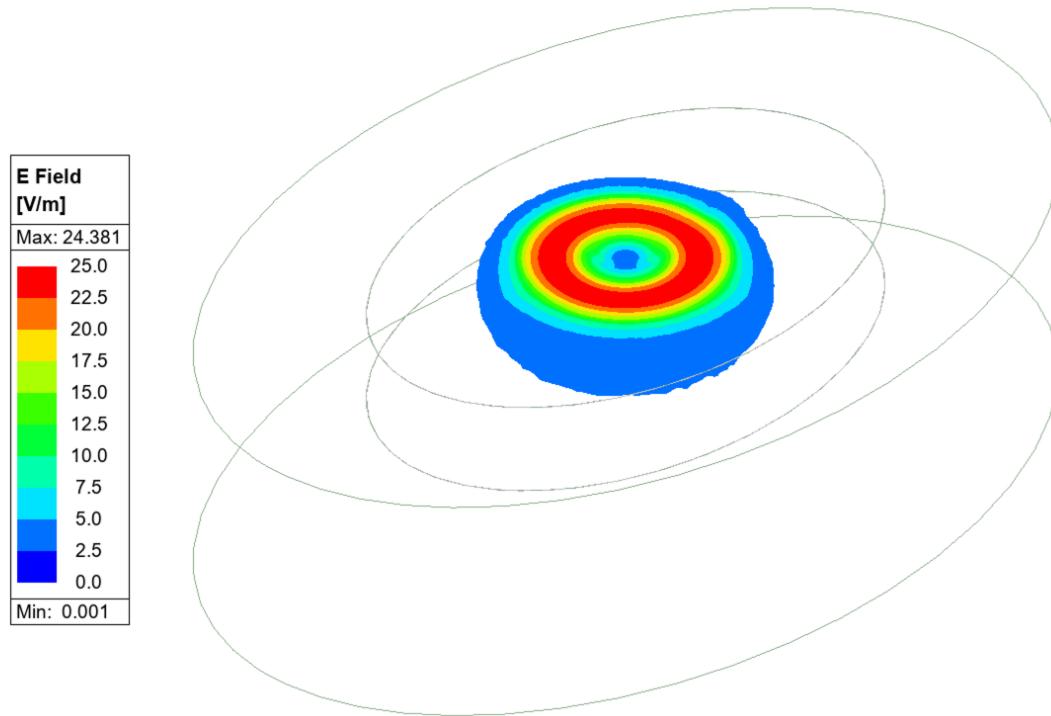
Figure 7: Peak E-field distribution inside phantom for direct exposure case

Summary

Based upon the above results, the accuracy of the SAR simulations is demonstrated by correlating H-field measurements to simulations. The validity of using this modeling and SAR computational method hence is established for iPhone models FCC IDs: A3260, BCG-E8948A; A3516, BCG-E8954A; A3517, BCG-E8955A; A3518, BCG-E8956A. Among, the exposure cases, the worst case peak spatial 1-gram averaged SAR of 0.031 W/kg and the highest peak spatial average E field (i.e., averaged over a cube of 2 mm x 2 mm x 2 mm) of 20.97V/m, is observed.

Overall, the SAR is significantly lower than the SAR limit of 1.6 W/kg (below 0.02 times the actual SAR limit). Therefore, we respectfully request that the allowance to use of this model to demonstrate RF Exposure compliance for Apple's proposed WPT products.

Annex A: Specific information for SAR computational modelling

1) Computation Resources

The models were simulated on a 48 core CPU server with an available RAM of 3 Terabytes. Each model variation took around 1.5 hours to complete. Based on the simulation profile, the minimum resources needed to finish these simulations will be approximately 8 core CPU with 512 GB of RAM. Using the minimum requirements simulation will likely take more time than 10 hours.

2) Algorithm implementing and validation

This section is divided into two parts. The code performance validation provides methods to determine that the finite-element algorithm in HFSS has been implemented correctly and works accurately within the constraints due to the finite numerical accuracy. It further determines the quality of absorbing boundary conditions and certain parts of the post processing algorithms that are part of HFSS. The second part has few canonical benchmarks. All benchmarks can be compared to analytical solutions of the physical problem or its numerical representation. The methods characterize the implementation of the finite-element algorithm used by HFSS in a very general way. They are defined such that it is not possible to tune the implementation for a particular benchmark or application without improving the overall quality of the code.

2.1) Code performance validation

2.1.1) Propagation homogeneous medium

A straight rectangular waveguide with ports on both ends is well suited as a first test of an implementation of the Finite-Element Method used by HFSS. The waveguide has a width of 20 mm, a height of 10 mm and a length of 300 mm. The waveguide is filled homogeneously with a material which, in three separate simulations, shall assume the following properties:

    i. $\varepsilon r = 1$, $\sigma = 0$ S/m;
    ii. $\varepsilon r = 2$, $\sigma = 0$ S/m;
    iii. $Re(\varepsilon r) = 2$, $\sigma = 0.2$ S/m.

To verify that the mesh used by HFSS is independent of orientation, the waveguide has been rotated so that it is not parallel with any principal coordinate plane (XY, XZ, YZ). The waveguide is driven in the TE10 mode at 10 GHz. Reported are the magnitudes of S21 and S11, as well as the values of the real and imaginary parts of the propagation constant γ. The following table provides the reference values [B1], acceptable result criteria, as well as the simulated results.

Table 4: Criteria for the waveguide evaluation

Re(ε_r)	1	2	2
σ	0	0	0.2
|S21| reference value	1	1	8.7×10^{-5}
Criterion for |S21|	≥ 0.9999	≥ 0.9999	$\pm 5 \times 10^{-6}$
|S21| simulated results	1	1	1.0×10^{-8}
|S11| reference value	0	0	0
Criterion for |S11|	≤ 0.003	≤ 0.003	≤ 0.003
|S11| simulated results	0.0008	0.00015	0.00008
Re(γ) reference value	0	0	31.17 m^{-1}
Criterion for Re(γ)	± 0.1 m^{-1}	± 0.1 m^{-1}	$\pm 2\%$
Re(γ) simulated results	0	0	31.174
Im(γ) reference value	138.75 m^{-1}	251.35 m^{-1}	253.28 m^{-1}
Criterion for Im(γ)	$\pm 2\%$	$\pm 2\%$	$\pm 2\%$
Im(γ) simulated results	138.75	251.351	253.277

As is seen in the above table, HFSS easily meets the criteria for properly and accurately calculating the waveguide problem.

2.1.2) Planar dielectric boundary

In order to test the reflection of a plane wave by a dielectric boundary, a rectangular waveguide can again be used. It is well known that the TE10 mode can be thought of as a superposition of two plane waves [1]. Each wave's direction of propagation makes an angle θ with the axis of the wave guide, given by

$$\cos^2\theta = 1 - (c/2af)^2 \tag{1}$$

where c is the speed of light, a is the width of the wave guide and f is the frequency. Assuming the axis of the waveguide is the Z axis and assuming the waveguide is filled with vacuum for Z>0 and filled with dielectric 1 with complex relative permittivity ε_r for Z<0, Fresnel reflection coefficients for the TE and the TM cases, defined as ratios of electric field strengths, are given by [2]

$$R^{TE} = (k_{0,z} - k_{1,z}) / (k_{0,z} + k_{1,z}) \tag{2}$$

$$R^{TM} = (\varepsilon_r k_{0,z} - k_{1,z}) / (\varepsilon_r k_{0,z} + k_{1,z}) \tag{3}$$

where $k_{0,z}$ and $k_{1,z}$ denote the z component of the propagation vector of the plane wave in vacuum and in the dielectric, respectively. They can be evaluated through

$$k_{0,z} = k_0 \cos\theta \tag{4}$$
$$k_{1,z} = k_0 \sqrt{(\varepsilon_r - \sin^2\theta)} \tag{5}$$

Finally, ε_r is complex and is given by

$$\varepsilon_r = Re(\varepsilon_r) - j\sigma/(2\pi f \varepsilon_0) \tag{6}$$

where $Re(\varepsilon_r)$ denotes the real part of the relative permittivity and σ is the conductivity of the medium.

For this test, a 20 mm × 10 mm waveguide with a length of 60 mm, as shown in Figure 8, was created. The top half was filled with vacuum and the bottom half with dielectric.
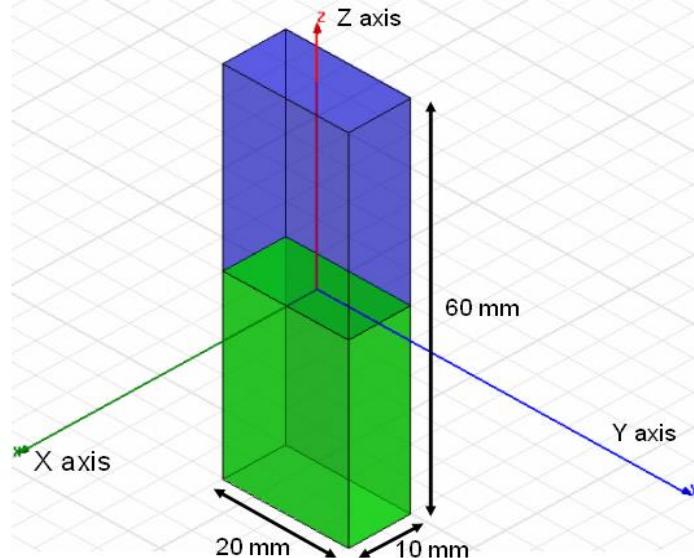

Figure 8: Waveguide filled half with vacuum and half with dielectric

In one copy of the model, all side walls were lossless metal, such that the dominant mode is the TE10 mode with propagation constant 138.75 m-1 at 10 GHz and represents the TE case in the reflection analysis. In the other copy of the model, the side walls that are parallel to the YZ plane were perfect magnetic conductors while the other walls were perfect electric conductors, such that the second mode (after a TEM mode which won't be used in this test) has propagation constant 138.75 m-1 at 10 GHz and represents the TM case in the reflection analysis.

Before simulation, the waveguides were rotated over an arbitrary angle such that no face is parallel with any coordinate plane. The waveguides were driven at 10 GHz in the proper mode. In doing so, it is good practice to calculate all propagating modes, but the coupling between modes is expected to be negligible. Simulations are performed for the cases of lossless and lossy dielectric. For the HFSS to pass the test, according to IEC 62704-1, the results need to be within 2% of the analytical values given in table below.

Table 5: Reflection at a dielectric interface

Re(εr)	σ (S/m)	RTE	RTE- Simulated	RTM	RTM - Simulated
4	0	0.4739	0.4739	0.1763	0.1763
4	0.2	0.4755	0.4755	0.1779	0.1779
4	1	0.5105	0.5105	0.2121	0.2121

As can be seen in above table, HFSS produces results that are identical to the analytical results.

2.2) Canonical Benchmarks

The results for few low frequency benchmarks are summarized below. These benchmarks were used to validate the accuracy of the tool at low frequencies:

2.2.1) Dipole Antenna:

The following parameter were used in the dipole antenna to resonate at 400KHz.

Dipole length: 375 meters
Feed gap: 2.5 meters
Dipole Diameter: 5 meters
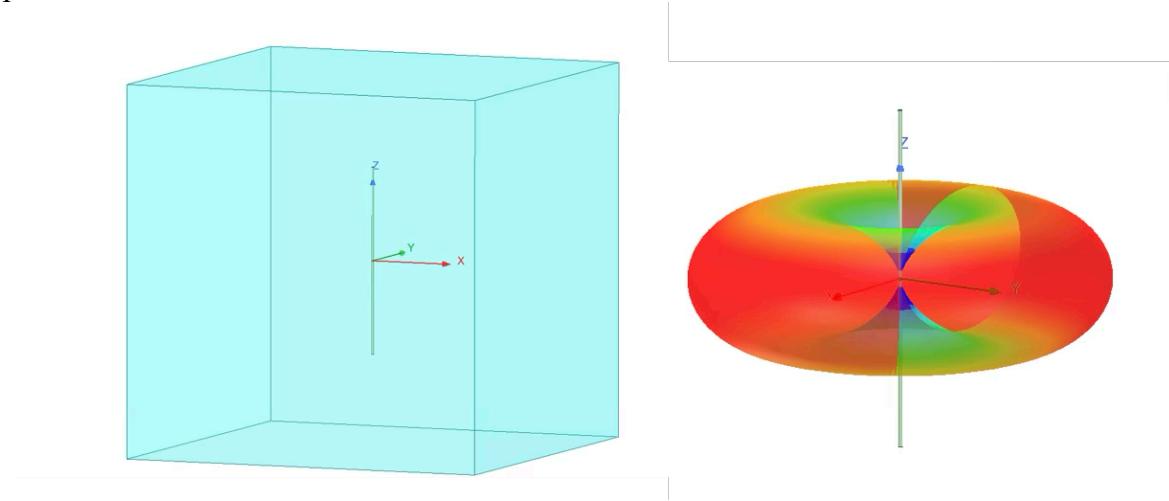
Figure 9: Dipole Antenna Model

The document IEC 62704-4 2020 was referenced to compare the tables. Two computation methods were demonstrated as shown below to show the validity of the model.

Table 6: Simulated dipole using FEM.

Quantity	Simulated Results	Tolerance	Satisfactory
Re(Z) @400 kHz	98.39 Ω		
Im(Z) @400 kHz	50.50 Ω		

Re(Z) @320 kHz	42.12 Ω	25 Ω < Re(Z) < 50 Ω	Yes
Im(Z) @320 kHz	-89.85 Ω	-50 Ω < Im(Z) < -100 Ω	Yes
Re(Z) @360 kHz	64.05 Ω	50 Ω < Re(Z) < 75 Ω	Yes
Im(Z) @360 kHz	-19.84 Ω	-25 Ω < Im(Z) < 0 Ω	Yes
Resonance Frequency Im(Z)=0	371.37 kHz	360 kHz < 380 kHz	Yes
Maximum power budget error	0.91 %	< 5 %	Yes

Table 7: Simulated dipole using MoM.

Quantity	Simulated Results	Tolerance	Satisfactory
Re(Z) @400 kHz	97.43 Ω		
Im(Z) @400 kHz	48.13 Ω		
Re(Z) @320 kHz	42.94 Ω	25 Ω < Re(Z) < 50 Ω	Yes
Im(Z) @320 kHz	-92.23 Ω	-50 Ω < Im(Z) < -100 Ω	Yes
Re(Z) @360 kHz	64.39 Ω	50 Ω < Re(Z) < 75 Ω	Yes
Im(Z) @360 kHz	-22.51 Ω	-25 Ω < Im(Z) < 0 Ω	Yes
Resonance Frequency Im(Z)=0	372.94 kHz	360 kHz < 380 kHz	Yes
Maximum power budget error	0.88 %	< 5 %	Yes

2.2.2) Toroid Inductor:

The parameters of the toroid are:

N = 20
R1 = 0.0136 m
R2 = 0.039 m
h= 0.025 m
μ_r = 64

The formula 14.16 below from [9] results in an inductance of 134.8 μH. The model created in HFSS resulted in an inductance of 137.25 μH at 1 MHz

$$ L = \frac{N\phi_m}{I} = \frac{\mu N^2 h}{2\pi} \ln \frac{R_2}{R_1} $$
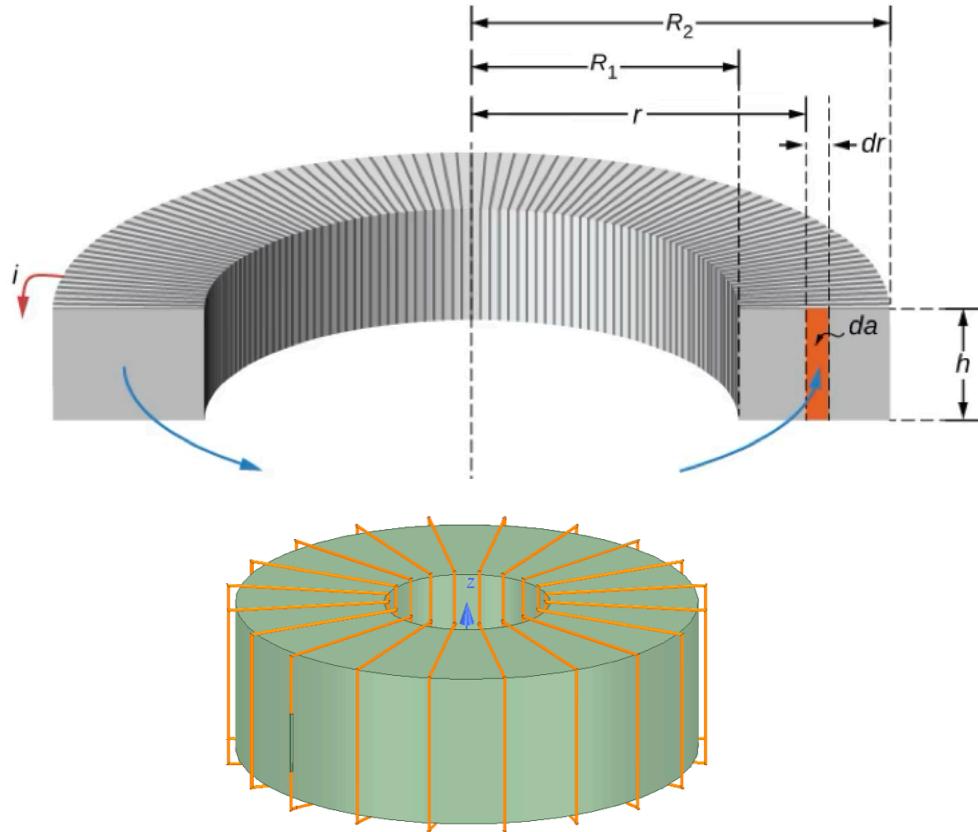
Figure 10: Toroid Model

2.2.3) Circular coil parallel to a flat, homogeneous phantom.:

The following benchmark is implemented using Equations 1-4 of the referenced Chen et al. (2014) paper. The analytical calculations using the reference resulted in 1.6 V/m, which matches the HFSS result shown in Figure 12.

Below is the coil and phantom parameters:

Coil Diameter: 50 mm
Number of Turns: 10
RMS Current: 0.707 A (Peak current = 1 A)
Frequency: 100 kHz
Coil-to-Body Distance: 5 mm
Tissue Conductivity: 0.05 S/m
Tissue Permittivity: 1120
Phantom radius: 84 mm
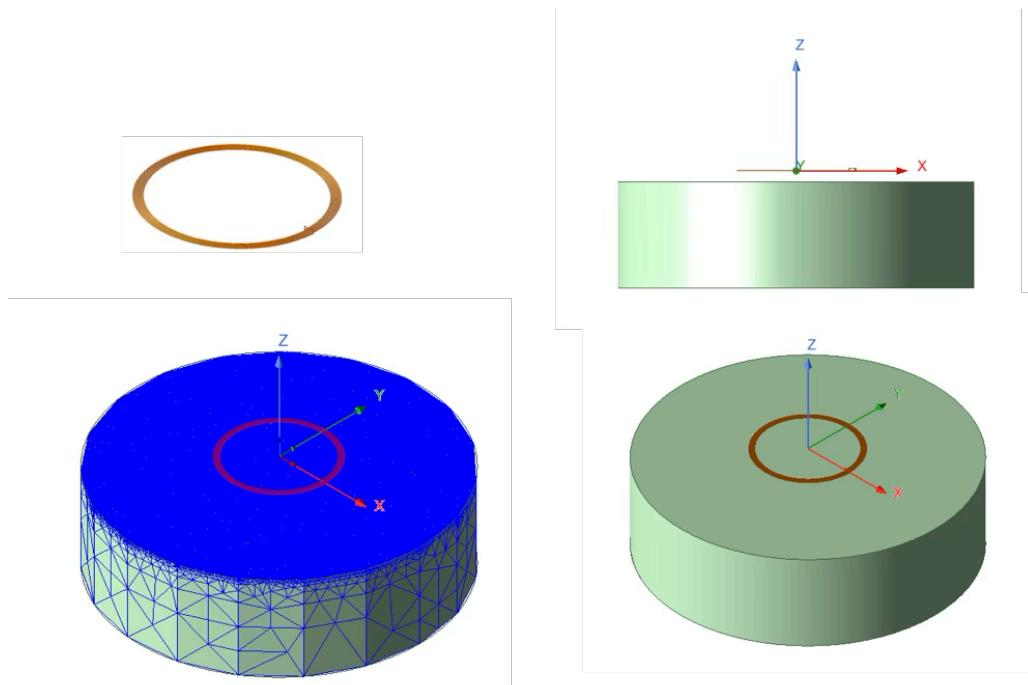
Figure 11: Current loop in front of a cuboid.

The simulated spatial peak RMS electric field in tissue is 1.55 V/m compared to the analytical 1.60 V/m.
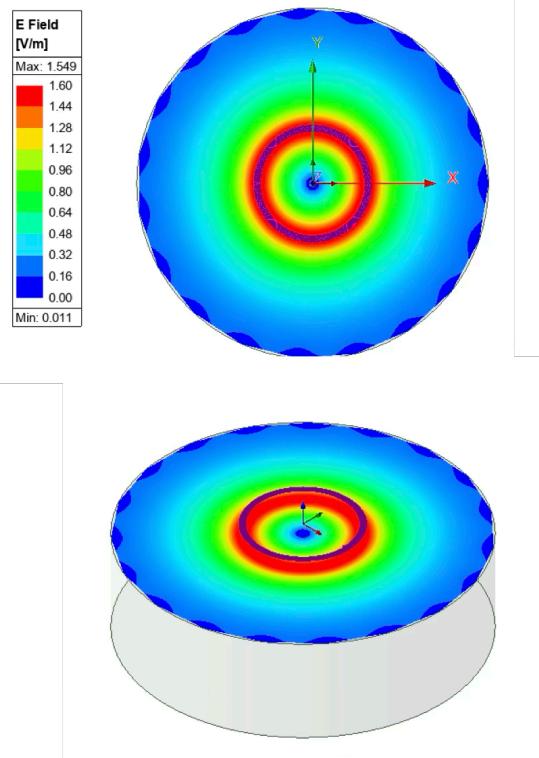

Figure 12: Electric Field plots at the phantom surface.

3) Computational peak SAR from peak components & One-gram averaged SAR procedure

The calculation method for SAR follows IEEE P1528.4. Once the solver calculated the S-Parameter results, different coils can be driven and the result from the S-Parameter calculation is automatically scaled to the driving current of the coils. This result combination provides the correctly scaled power loss density in the phantom. The SAR calculation computes the local SAR first using electric field and conducting current:

$$SAR = \vec{E} \bullet \vec{J}_{conj}/(2\rho)$$

Afterwards the local SAR is averaged over a specific mass, usually 1g or 10g. As described in [IEEE P1528.4] the mass averaging is done by mapping the results to a structured hexahedral grid and afterwards the averaging scheme for FDTD per [IEEE P1528.4] is applied. The SAR calculation on the hexahedral grid is compliant with IEC 62704-1.
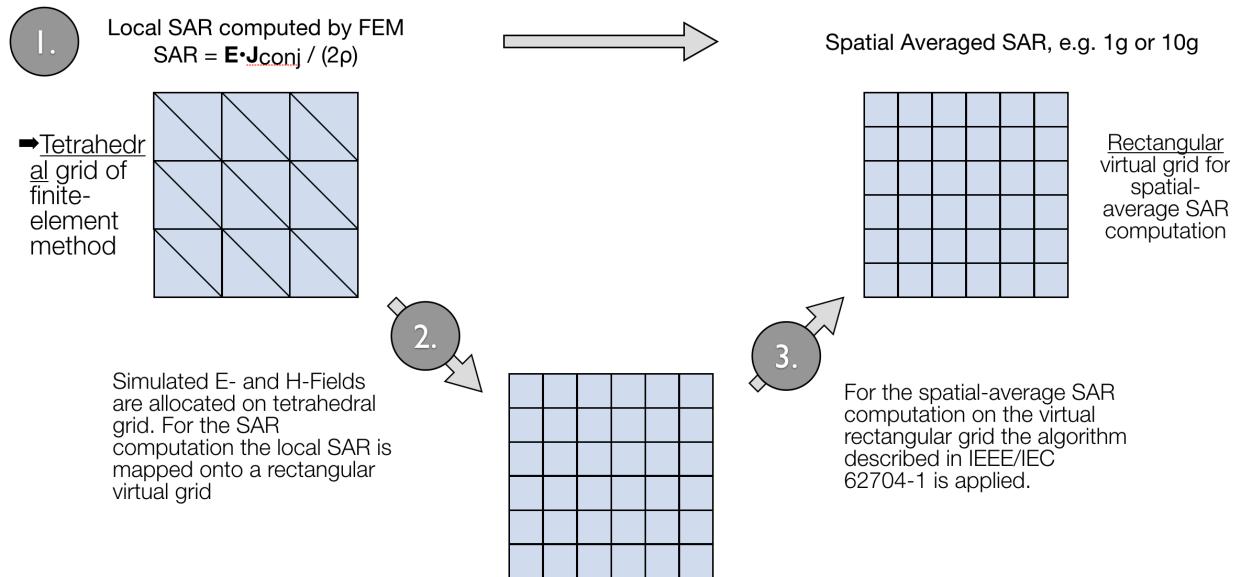
Figure 13: IEEE P1528.4 for SAR computation

4) Total Computational Uncertainty

Below is a table summarizing the budget of the uncertainty contributions of the numerical algorithm and of the rendering of the simulation setup. The table was filled using the IEC 62704-4, 2020. For the simulations, the extreme case where the phantom is placed directly in front of the Phone is considered. As the phantom with reference dielectric parameters are used (as described in section 5); the corresponding phantom dielectric uncertainty is set to zero (section 7.2.6, IEC 62704-4, 2020).

Table 8: Budget of uncertainty contributions of the numerical algorithm (filled based on IEC 62704-4 2020).

a	b	d	e	g
Uncertainty component	Subclause	Probability distribution	Divisor f(d, h)	Uncertainty %
Mesh resolution	7.2.2	N	1	0.18
ABC	7.2.3	N	1	0.01
Power budget	7.2.4	N	1	0.00
Convergence	7.2.5	R	1,73	0.12
Phantom dielectrics	7.2.6	R	1,73	0.00
Combined standard uncertainty (*k* = 1)				**0.40**

Below is a table summarizing the budget of the uncertainty of the developed model of the DUT so far. The table was filled using the IEC 62704-4, 2020.

Table 9: Uncertainty of DUT Model

a	b	d	e	g
Uncertainty component	Subclause	Probability distribution	Divisor f(d, h)	Uncertainty %
Uncertainty of the DUT model (based on near field distribution)	7.3.2	N	1	2.44
Uncertainty of the measurement equipment and procedure	7.3.3	N	1	7.6
Combined standard uncertainty (*k* = 1)				**7.98**

The expanded (K=2) uncertainty result as per the IEC/IEEE 62704-1, 2017 and IEC/IEEE 62704-4, 2020 is listed in Table 9. The expanded standard uncertainty is 15.96%, which is lower than the limit of 30.

Table 10: Expanded Standard Uncertainty

a	b	c	d	e	f	g	h
Uncertainty component	Sub clause	Tolerance %	Probability distribution	Divisor f(d,h)	c_i	Uncertainty %	v_i or v_{eff}
Uncertainty of the test setup with respect to simulation parameters	7.2		N	1	1	0.40	
Uncertainty of the developed numerical model of the test setup	7.3		N	1	1	7.98	
Combined standard uncertainty ($k = 1$)						**7.98**	
Expanded standard uncertainty ($k = 2$)						**15.96**	
Columns c, g and h shall be filled in based on the results of Table 11 and Table 12							
NOTE 1 Column headings a to h are given for reference							
NOTE 2 Abbreviation used in Table 8, 9, 10:							
N – normal probability distribution							
R – rectangular probability distribution							
NOTE 3 The divisor is a function of the probability distribution and degrees of freedom (v_i and v_{eff})							
NOTE 4 c_i is the sensitivity coefficient that is applied to convert the variability of the uncertainty component into a variability of SAR							

The properties of the key materials of the DUT, as well as their tolerances, are listed in the following table.

Table 11: Material Properties and Tolerances

	Permittivity +/- Tolerance	Permeability +/- Tolerance	Loss Tangent +/- Tolerance	Conductivity +/- Tolerance
TX Ferrite	1	1345 +/-134	0	0
RX Ferrite	1	3300 +/-825	0	0
TX Coil	1	1	0	5.8e7 +/- 5.8e5
RX Coil	1	1	0	5.8e7 +/- 5.8e5
TX Shield	1	1	0	6.1e7 +/- 6.1e5
RX Shield	1	1	0	5.8e7 +/- 5.8e5

References:

1) IEC/IEEE 62704-4, 2020: "Determining the peak spatial-average specific absorption rate (SAR) in the human body from wireless communication devices, 30 MHz to 6 GHz – Part 4: General requirements for using the finite element method for SAR calculations."

2) IEC/IEEE 62704-1, 2017: "Determining the peak spatial-average specific absorption rate (SAR) in the human body from wireless communications devices, 30 MHz to 6 GHz - Part 1: General requirements for using the finite difference time-domain (FDTD) method for SAR calculations."

3) The electrical conductivity of human cerebrospinal fluid at body temperature, S.B. Baumann ; D.R. Wozny ; S.K. Kelly ; F.M. Meno, IEEE Transactions on Biomedical Engineering (Volume: 44 , Issue: 3 , March 1997)

4) https://itis.swiss/virtual-population/tissue-properties/database/thermal-conductivity/

5) C.Gabriel, S.Gabriel and E.Corthout: The dielectric properties of biological tissues: I. Literature survey, Phys. Med. Biol. 41 (1996), 2231-2249.

6) S.Gabriel, R.W.Lau and C.Gabriel: The dielectric properties of biological tissues: II. Measurements in the frequency range 10 Hz to 20 GHz, Phys. Med. Biol. 41 (1996), 2251-2269.

7) S.Gabriel, R.W.Lau and C.Gabriel: The dielectric properties of biological tissues: III. Parametric models for the dielectric spectrum of tissues, Phys. Med. Biol. 41 (1996), 2271-2293.

8) X. L. Chen et al., "Human Exposure to Close-Range Resonant Wireless Power Transfer Systems as a Function of Design Parameters," in IEEE Transactions on Electromagnetic Compatibility, vol. 56, no. 5, pp. 1027-1034, Oct. 2014.

9) Frederick Terman., "Radio Engineer's Handbook", McGraw-Hill.